Document downloaded from:

http://hdl.handle.net/10251/66078

This paper must be cited as:

Galindo, J.; Tiseira Izaguirre, AO.; Navarro García, R.; López Hidalgo, MA. (2015). Influence of tip clearance on flow behavior and noise generation of centrifugal compressors in near-surge conditions. International Journal of Heat and Fluid Flow. 52:129-139. doi:10.1016/j.ijheatfluidflow.2014.12.004.

The final publication is available at

http://dx.doi.org/10.1016/j.ijheatfluidflow.2014.12.004

Copyright Elsevier

Additional Information

Influence of tip clearance on flow behavior and noise generation of centrifugal compressors in near-surge conditions

J. Galindo, A. Tiseira, R. Navarro*, M. A. López

CMT - Motores Térmicos, Universitat Politècnica de València
Camino de Vera, 46022 Valencia

Abstract

CFD has become an essential tool for researchers to analyze centrifugal compressors. Tip leakage flow is usually considered one of the main mechanisms that dictate compressor flow field and stability. However, it is a common practice to rely on CAD tip clearance, even though the gap between blades and shroud changes when compressor is running. In this paper, sensitivity of centrifugal compressor flow field and noise prediction to tip clearance ratio is investigated. 3D CFD simulations are performed with three different tip clearance ratios in accordance to expected operating values, extracted from shaft motion measurements and FEM predictions of temperature and rotational deformation. Near-surge operating conditions are simulated with URANS and DES. DES shows superior performance for acoustic predictions. Cases with reduced tip clearance present higher pressure ratio and isentropic efficiency, but no significant changes in compressor acoustic signature are found when varying clearance. In this working point, tip clearance is immersed in a region of strongly swirling backflow. Therefore, tip leakage cannot establish any coherent noise source mechanism.

Keywords: CFD Simulation, Turbocharger, Shaft motion, aeroacoustics, DES, URANS

*Corresponding author. Tel.: +34 963 877 650

Email addresses: galindo@mot.upv.es (J. Galindo), anti1@mot.upv.es (A. Tiseira), ronagar1@mot.upv.es (R. Navarro), milpehi@mot.upv.es (M. A. López)

1. Introduction

Turbochargers are present in almost all diesel engines and its use in gasoline engines has been steadily increasing in the last years. Turbocharging allows reductions of engine displacement and weight without reducing the power and torque produced, in a trend known as downsizing. This approach reduces fuel consumption and emissions, which is a must for successfully fulfilling the current regulations.

Yet strongly downsizing of engines and increase of low speed torque raises an issue with turbocharger airborne noise [1], since compressor operating points are shifted towards surge region [2].

Leakage flow from blade PS to SS across tip clearance is often considered as a key point in the stability and noise production of centrifugal compressors. Raitor and Neise [3] conducted an experimental study to analyze the sound generation mechanisms of centrifugal compressors. Tip clearance noise (TCN) predominates over BPF tone for subsonic flow conditions at low compressor speeds. TCN is a narrow-band noise observed at frequencies about half the blade passing frequency (BPF), which increase with speed. Raitor and Neise considered that secondary flow through blade tip clearance is the source of TCN.

In this frame, CFD is a tool used by researchers to investigate centrifugal compressor flow field and particularly tip leakage flow.

Mendonça et al. [4] analyzed flow-induced aeroacoustics of an automotive radial compressor using DES. A narrow band noise at a frequency about 70% of rotational speed was detected. Rotating stall was found to be the source of the narrow band noise. Tip leakage allows the stalled passages to recover by pushing the low momentum region to the rotation-trailing passage, according to Mendonça et al.

Tomita et al. [5] studied two compressors with similar map except in surge vicinity. Unsteady pressure measurements performed just upstream the impeller leading edge at low mass flow rate revealed differences between compressors: the one with the narrowest operating range showed large pressure fluctuations at subsynchronous speeds moving circumferentially at about 50%-80% of compressor speed, whereas compressor with wide operating range did not exhibit this large amplitude fluctuations. 3D CFD numerical simulations were also performed in order to analyze fluid phenomena at this low mass flow rate conditions. Compressor with less surge margin presented a tornado-type vortex between blades, blocking the incoming flow. This vortex

is convected downstream and a new one is created in the adjacent blade, in a rotating stall pattern. Conversely, spiral-type tip leakage vortex breakdown occurred at all blades for compressor with higher surge margin. Some rotating instability was observed in this compressor, but not as severe as the rotating stall experienced as in the other compressor. Tomita et al. [5] concluded that tip leakage vortex breakdown could stabilize the flow structure and thus increase surge margin.

Increased computational resources have made possible to include tip clearance in most of the current CFD simulations of centrifugal compressor [4, 5]. However, compressor geometry is often obtained from reverse engineering or manufacturer's CAD, thus modeling a *cold* tip clearance that is not representative of actual working conditions. Deformations due to temperature, rotation or pressure are usually neglected, and shaft motion is not considered. Including these effects will led to coupled fluid-structure simulations, which are very expensive. Nevertheless, the effect of these factors should be studied to assess the validity of simulations using CAD clearance.

Many researchers have performed studies of tip clearance sensitivity on global variables and local flow features.

Danish et al. [6] conducted a numerical study in which overall performance and flow field were investigated for nine tip clearance levels from no gap to 16% tip clearance ratio (TCR). Numerical simulations were performed with frozen rotor technique. Two different clearance increase approaches were used: reduction of blade height while keeping same housing dimensions and increase of shroud diameter with same blade height. For operating conditions close to best efficiency point, maximum increase of TCR by decrease of blade height caused a loss of 15% in pressure ratio and 10% in efficiency. If shroud size is increased instead, pressure ratio is reduced by 13% and efficiency by 8.5%.

Jung et al. [7] performed steady simulations using the same impeller with six different tip clearance profiles. Reductions in tip clearance caused an increase in pressure ratio and efficiency. Particularly, a decrease in tip clearance at the trailing edge improved the compressor performance more than implementing the same reduction in leading edge tip clearance. A reduced tip leakage flow was found to significantly improve the diffusion process downstream the impeller.

Measurements performed by Wang et al. [8] indicated that variations of tip clearance caused small influence on stall inception. However, the reasons could not be investigated because their mixing-plane, steady simulations

failed to converge at near surge conditions.

However, in these sensitivity studies, particular TCRs are not usually justified by expected values of compressor actual working conditions and effect on noise generation is not assessed.

According to the literature review, tip leakage flow may play a role in noise generation and stability of centrifugal compressors. CFD can provide a deeper insight into the issue, but clearance sensitivity to noise generation must be first assessed to decide if clearance variations from baseline CAD conditions can be safely neglected. In such a sensitivity study, TCRs should be set in accordance to expected values while compressor is operating.

In this paper, the effect of tip clearance size on fluid flow and noise spectra of a 49 mm exducer diameter turbocharger compressor is studied. Section 2 is devoted to the estimation of tip clearance reduction during actual compressor operation. In Section 3, the numerical set-up is described and the approach to perform the clearance sensitivity analysis is explained. Tip clearance size impact on global variables and noise generation is evaluated in Section 4 by means of PSD comparison. Flow field is investigated in Section 5 in order to explain the spectra obtained by different TCRs. Finally, Section 6 includes the main findings of the paper.

2. Estimation of actual tip clearance

In Section 1, some effects usually not considered when simulating turbocharger compressors were introduced. For the sake of accuracy, a two-way coupled fluid-structure simulation should be performed to take into account potential aeroelastic effects, along with impeller and housing deformations caused by temperature, rotation and pressure differences. However, this approach would lead to unaffordable computational times.

Wang et al. [8] used a two-step calculation procedure to take into account impeller deformation when simulating centrifugal compressor flow, avoiding a two-way coupled fluid-structure simulation. First, the deformation of the compressor blades were simulated with finite element method (FEM). Then, the flow field was recalculated with the deformed impeller estimated with FEM. In this way, tip clearance changed from a uniform clearance ratio of 7.3% into a non-uniform profile that presents greater reduction with increasing meridional coordinate (TCR is 50% larger at the leading edge than at the trailing edge). Moreover, incident and exit blade metal angles were also deformed. Particularly, tip outlet angle at trailing edge increased 3.5°. Leakage

flowrate is thus affected by impeller deformation, over all at trailing edge.

In this paper, sensitivity of TCR to centrifugal compressor aeroacoustics will be first investigated. Aeroelasticity is neglected because centrifugal compressor blades are not as long and slender as in their axial counterparts, which do suffer from phenomena such as flutter. Deformation due to thermal and pressure loads and centrifugal forces can be taken into account with a one-way fluid-mechanical simulation. If noise happens to be highly dependent on TCR, the flow field should be recalculated with the actual tip clearance geometry, following the approach of Wang et al. [8].

Besides, dynamic mesh approach should be employed to consider the complex shaft motion pattern described (see for example the explanation of Nelson [9]). This would imply a great increase in computational effort compared to traditional sliding mesh technique, in which rotor region is meshed only once and it is rotated across sliding interfaces, in accordance with compressor speed. The possible effect of shaft precession on noise generation is thus neglected in this paper. Instead, eccentricity measurements are performed in Section 2.2 to assess maximum clearance reduction due to shaft motion, so as to be considered in the subsequent sensitivity analysis.

2.1. Thermal and rotational deformation

To estimate decrease of tip clearance due to impeller deformation, mean wheel temperature (120°C) predicted by CFD and rotational speed (160 krpm) were used as an input to a structural simulation with FEM, which computed the nodal displacement. The impeller is meshed with more than 12000 quad/tri elements. The equations are then solved using the preconditioned conjugate gradient solved implemented in ANSYS Structural.

Pressure deformation was not considered because its contribution to impeller deformation is marginal [8]. Selection of mean value instead of temperature distribution is justified by high thermal diffusivity of aluminum, which is the material of most compressor wheels [10]. The simulation was done with characteristics of the Aluminum Alloy (density = 2770 $^{kg}/_{m^3}$, Young's Modulus = 71 GPa).

Figure 1 shows the total deformation of the compressor wheel. Maximum deformation of the inducer blades is 11% of CAD tip clearance.

2.2. Eccentricity due to shaft motion

In order to estimate the tip clearance variation due to shaft motion, the technique developed by Pastor et al. [11] is applied. It consists in an im-

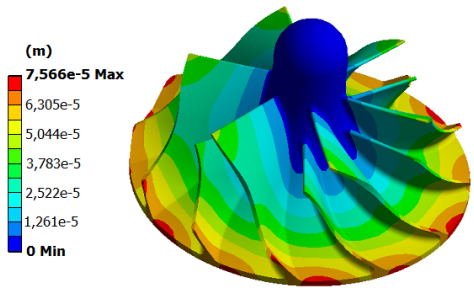

Figure 1: Impeller deformation due to rotational and thermal loads.

age recording methodology with a processing algorithm to estimate the shaft motion. Pastor et al. [12] showed that this technique requires a less intrusive apparatus than infrared sensor measurements, also providing direct observation of shaft motion phenomenon. Galindo et al. [13] used this methodology to improve the knowledge of the behavior of the turbochargers in critical conditions of lubrication, because, as López [14] indicated, image recording is better suited than standard inductive sensors for shaft motion measurements in these lubrication conditions. For more details, please refer to the work of López [14].

Figure 2 depicts the layout of the image recording apparatus. The camera is placed in front of the turbocharger on the compressor side, positioning it as coaxial as possible to the turbocharger shaft and focused to the shaft tip. A 90° elbow is attached at the inlet of the compressor housing with a glass window to allow the proper display of the shaft through the camera. Images are taken with a PCO Pixelfly 12-bit CCD Camera with spatial resolution of 1280x1024 pixels. The distance between the compressor and the camera is approximately 300 mm. The resolution obtained with this layout is approximately 5 μm per pixel. This resolution allows the observation of shaft movements.

The processing algorithm consists on differentiating specific zones of the image in order to obtain their coordinates. Two screws are placed at the impeller's eye plane (see Fig. 3). They are used as reference points to calculate the relative position of the shaft, avoiding errors due to structural vibrations. Figure 3 shows a photograph of the shaft motion. The impeller's eye can be seen along with the reference points (left and right screws). The processing algorithm identifies the shaft tip and its center (in blue in Fig. 3), whose

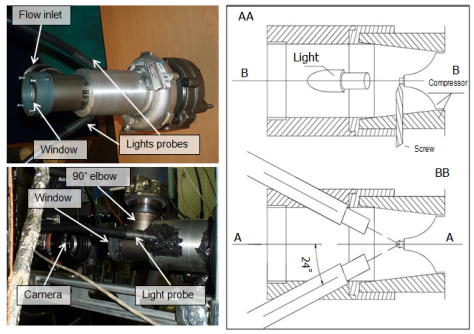

Figure 2: Camera layout for shaft motion observation.

coordinates are calculated using the reference points for the subsequent determination of the shaft motion.

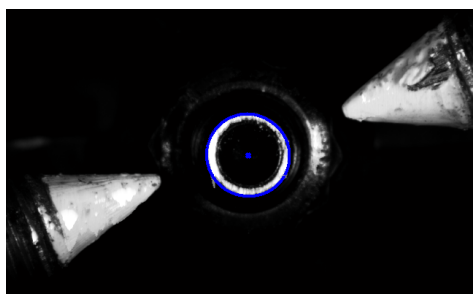

Figure 3: Photograph of shaft motion, showing the estimated position of the shaft center.

The maximum eccentricity of the turbocharger is obtained by manually achieving the physical limit of shaft motion. Figure 4 shows the maximum eccentricity (ellipse with solid black line) and the shaft motion at 160 krpm (blue dot markers). The shaft motion describes a zone with a radius between 100 μm and 150 μm regarding the center of the impeller's plane eye. This motion represents a 22% to 34% of reduction of the original clearance. Therefore, the maximum reduction of the original tip clearance is between 33% to 45%.

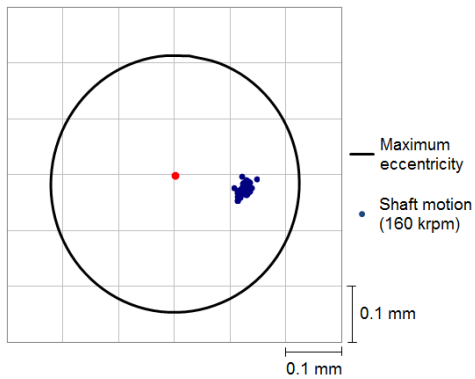

Figure 4: Shaft motion at 160 krpm.

3. Numerical Model

3.1. Domain and numerical set-up

The impeller, vaneless diffuser and volute of the compressor were digitalized. A structured-light 3D scanner provided a point cloud of the bodies, which were processed by reverse engineering software to reconstruct smooth surfaces. In order to avoid influence of manufacturing variability, only one main blade and one splitter blade were digitalized, creating the rest by revolution. The impeller and the diffuser are thus 360° modeled. Backplate cavity along with (cold) tip clearance are also provided by the digitalization process. In addition, inlet and outlet cross sections were extruded 5 diameters long to obtain the CFD domain shown in Fig. 5. The full domain (inlet pipe, impeller, hub cavity, vaneless diffuser, discharge volute and outlet duct) is meshed with 9.5 million polyhedral cells. Navarro [15] performed a mesh independence analysis, showing that a mesh twice as fine does not provide significant differences in terms of global variables and noise predictions.

Rigid body motion approach was employed for the computations, in which heat transfer with the surroundings was neglected. Smooth walls were considered. Fixed outlet pressure, constant compressor speed of about 160 krpm and mass flow rate corresponding to 1.4 times surge mass flow at this compressor speed were set to represent a near-stall operating condition. Second-order accurate transient solver was used with a time-step size so that the impeller mesh turns 1° per time step, since Navarro [15] proved that this time-step is sufficient to accurately resolve pressure spectra within human hearing range.

Turbulence modeling plays an important role in flow field and noise prediction of a centrifugal compressor, particularly at near-surge conditions. In this paper, Direct Numerical Simulations (DNS) are rejected due to their infeasibility in terms of computational cost. In order to predict compressor aeroacoustics, three approaches to model turbulence could be thus considered: Unsteady Reynolds Averaged Navier Stokes Simulations (URANS), Detached Eddy Simulation (DES) or Large Eddy Simulation (LES).

LES are often used in computational aeroacoustics (CAA) [16], due to their potential to capture broadband noise turbulent sources. Dufour et al. [17] reviewed some works using large eddy simulations for predicting turbomachinery flow. By looking at their survey, it can be concluded that LES is much more extended in axial turbomachinery than in their radial counterparts. To the authors' knowledge, LES in turbocharger compressors have only been covered by Karim et al. [18] and the set of works performed by researchers from KTH and University of Cincinnati. Hellström et al. [19, 20], Jyothishkumar et al. [21] and Semlitsch et al. [22] reported good agreement between their large eddy simulations and experimental measurements, showing the potential of LES to predict centrifugal compressor flow behavior, particularly at near-surge conditions. However, LES is not considered in this paper due to the computational cost that would imply using a LES-suited grid.

In this work, URANS simulations are performed with $k-\omega$ SST model [23] closure model. This model is very suited for compressors, for its accuracy in

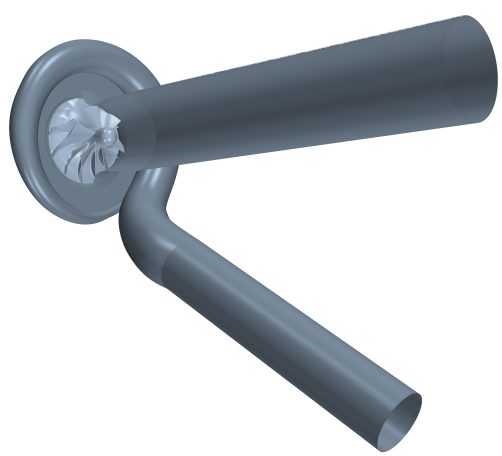

Figure 5: CFD domain.

predicting flow with adverse pressure gradients. Menter et al. [24] applied the SST model for different turbomachinery cases, for which a good agreement against experimental measurements was found. The model proved to be good at capturing usual turbomachinery flow features such as flow separation, swirl or strong flow mixing. Robinson et al. [25] also used the aforementioned turbulence model to analyze the influence of the spacing between impeller and vaned diffuser in a centrifugal compressor. Smirnov et al. [26] applied the $k-\omega$ SST model for the calculation of flow in a one-stage centrifugal compressor with a vaned diffuser. Good agreement of the computed velocity field with the measurements data at the impeller exit is obtained by Smirnov et al. Downstream of the diffuser vane, prediction quality depends on the operating point. A comparison between turbulence models was done at one operating point. The SST model provided better agreement with experimental data than $k-\epsilon$ and $k-\omega$ models.

Finally, DES model is an hybrid RANS-LES approach in which the boundary layer is modeled using URANS and LES is employed for the free stream detached flow. With such a blending between turbulence approaches, DES is intended to save computational cost when compared with LES but retaining some of the eddy-resolving capabilities, with the corresponding improvement in broadband noise predictions regarding URANS. For this reason, DES model is also used in this paper, although it is still not very popular in turbomachinery simulations. Tucker [27] listed 40 turbomachinery cases with eddy-resolving turbulence models, only 3 of them being hybrid RANS-LES. In this work, DES will be performed in combination with a SST $k-\omega$ turbulence model, "which functions as a sub-grid-scale model in regions where the grid density is fine enough for a large-eddy simulation, and as a Reynolds-averaged model in regions where it is not" [28]. Low-Reynolds number near-wall resolution is used, since Mendonça et al.[4] showed that this approach improved the prediction of the compressor map compared to experimental measurements when using steady-state RANS $k-\omega$ SST simulations. Particularly, IDDES [29, 30] is used, which combines WMLES and DDES hybrid RANS-LES approaches. Mockett [31] studied several DES models, concluding that IDDES extended the range of suitable applications of DDES, by reducing the issue with log-layer mismatch (LLM). The mesh used in this paper may not be fine enough to take advantage of the WMLES branch in IDDES, but at least this turbulence model should perform as DDES. Van Rennings et al. [32] used DDES for simulations of an axial compressor near stall. Imposed geometrical periodicity was found to affect large scale turbu-

lent structures, concluding that the full compressor should be modeled for the sake of accuracy.

Simulations using URANS and DES turbulence approaches were performed using the segregated solver of Star-CCM+ [33]. DES results using the described model has been already validated against experimental measurements for aeroacoustic purposes by Broatch et al. [34]. Navarro [15] showed that LES mode of detached eddy simulations is present in the core of the rotor passages and the recirculating flows upstream the impeller. A comparison between predicting capabilities of URANS and DES will be performed in Section 4.

3.2. Tip clearance reduction approach

In Section 2, a maximum clearance reduction of 45% is estimated. In order to assess compressor performance indicators, flow features and noise production sensitivity to tip clearance, three levels are considered: original (CAD) clearance, 2/3 of original clearance and 1/3 of original clearance. In this way, expected clearance reduction range is comprised in the sensitivity analysis.

Tip clearance reduction can be done with two opposed approaches, either increasing impeller size or decreasing shroud diameter. Impeller increase would mimic temperature and rotational deformation, but tip clearance reduction due to shaft motion represents an approximation regardless of the method used. However, unrealistic deformation of impeller geometry may impact flow behavior more than subsequent reduction of tip clearance. In this paper it is thus preferred to keep impeller size and reduce the shroud to obtain the desired TCRs. In any case, Danish et al. [6] proved that these two approaches to change tip clearance yield similar results.

The reduction of shroud that causes the three different TCRs studied in this paper can be observed in the left-hand side of Fig. 6. The three meshes produced with this approach present a similar amount of elements, being about 9.5 million polyhedral cells.

4. Comparison of overall performance and acoustic signatures

4.1. Experimental setup

Aside from the numerical comparison between turbulence models and different TCRs, experimental spectra are used as a reference. The experimental measurements shown in this paper were obtained installing a turbocharger

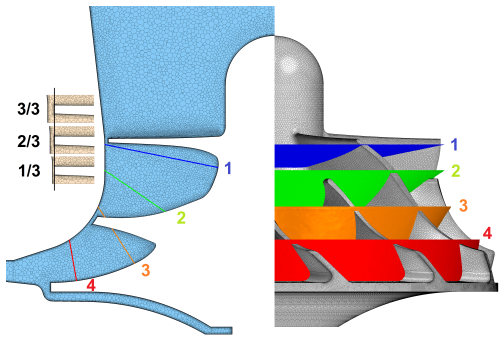

Figure 6: Rotor region mesh: cross-section (left) and impeller (right), including a close-up of tip clearance for the cases studied and isomeridional surfaces.

test rig in an anechoic chamber. A detailed description of the gas stand is given by Galindo et al. [35].

Long, straight pipes were placed at the inlet and outlet of the compressor, as depicted in Fig. 7. Position of piezoelectric pressure sensor arrays are also included in the sketch. These probes were used to sample pressure signals at 100 kHz during 1 second at the desired operating condition, using a Yokogawa digital oscilloscope.

Inlet and outlet linear arrays of three piezoelectric sensors each were designed in accordance with Piñero et al. [36], to take advantage of their beamforming-based signal analysis method to decompose pressure signals into a forward-traveling wave $p_{forw}(t)$ and a backward-traveling wave $p_{back}(t)$.

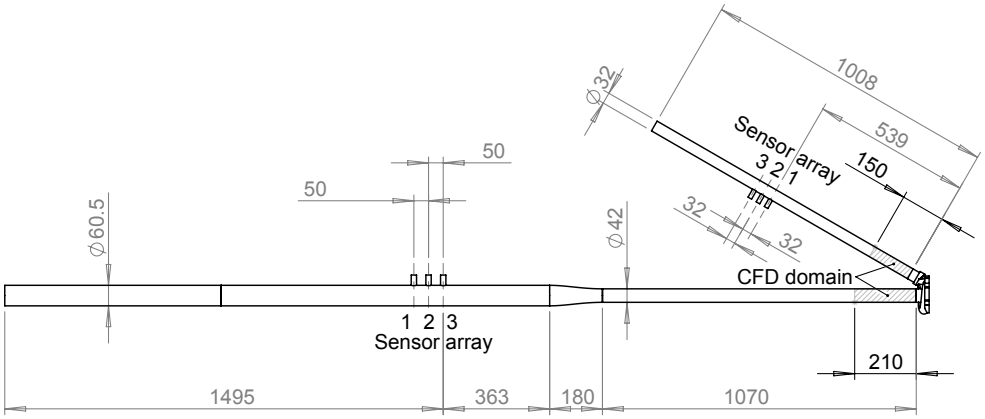

Figure 7: Compressor piping layout, highlighting the CFD domain and the sensor arrays.

A full description of the experimental apparatus used to obtain the acoustical measurements is presented by Broatch et al. [34].

4.2. Compressor performance variables

In first place, compressor global variables are compared. Total-to-total pressure ratio, specific work and isentropic efficiency,

$$\begin{aligned} \Pi_{t,t} &= \frac{p_{out,0}}{p_{in,0}} \\ W_u &= \frac{\dot{W}}{\dot{m}} = \frac{\frac{2\pi N(rpm)}{60}\tau}{\dot{m}} = c_p(T_{out,0} - T_{in,0}) \\ \eta_s &= \frac{\dot{W}_s}{\dot{W}} = \frac{T_{in,0}\left(\Pi_{t,t}^{\frac{\gamma-1}{\gamma}} - 1\right)}{T_{out,0} - T_{in,0}}, \end{aligned} \tag{1}$$

are either experimentally measured or numerically calculated. Table 1 includes these global variables along with relative difference against experimental measurements and relative difference against CAD clearance case with the corresponding turbulence model, defined as:

$$\epsilon_{exp}(\%) = \frac{\phi_{CFD} - \phi_{exp}}{\phi_{exp}} \cdot 100 \quad \epsilon_{3/3}(\%) = \frac{\phi_{CFD} - \phi_{CFD,3/3}}{\phi_{CFD,3/3}} \cdot 100. \tag{2}$$

For both turbulence approaches, cases with original clearance provide compressor performance values closer to experimental results than cases with reduced clearance. Decreasing tip gap improves compressor isentropic efficiency and pressure ratio. In URANS simulations, a reduction of TCR slightly increases specific work, but in DES there is not a monotonous trend.

URANS case with CAD clearance predicts compressor performance parameters showing better agreement with experimental measurements than DES, particularly in terms of isentropic efficiency. However, a better estimation of global variables does not necessarily imply that URANS is more accurate than DES in predicting compressor noise generation, as the next section will prove.

Table 1: Compressor global variables measured in the experimental test rig and predicted by the numerical model. In each box, the value is followed by the relative difference against experimental measurements and the relative difference against CAD clearance case with the corresponding turbulence model.

Case		$\Pi_{t,t}$ [-] ($\phi/\epsilon_{exp}/\epsilon_{3/3}$)	W_u [$kJ \cdot kg^{-1}$] ($\phi/\epsilon_{exp}/\epsilon_{3/3}$)	η_s [%] ($\phi/\epsilon_{exp}/\epsilon_{3/3}$)
Exp.		2.22/–/–	121/–/–	62.2/–/–
URANS	3/3	2.21/-0.5/–	122/0.7/–	62.3/0.1/–
	2/3	2.26/1.7/2.2	123/1.2/0.5	63.9/2.7/2.6
	1/3	2.31/4.1/4.7	124/2.2/1.5	65.3/5.0/4.9
DES	3/3	2.23/0.4/–	122/0.6/–	63.2/1.6/–
	2/3	2.27/2.1/1.6	122/0.1/-0.5	65.0/4.4/2.8
	1/3	2.32/4.2/3.8	122/0.7/0.1	66.5/6.8/5.1

4.3. Compressor acoustic spectra

In order to assess the effect of tip clearance on centrifugal compressor noise, the methodology developed by Broatch et al. [34] is followed. Experimental signals were sampled during 1 s, whereas numerical monitors were stored at each case for more than 50 ms (corresponding to 140 impeller revolutions) after reaching a steady state in terms of global variables. Welch's overlapped segmented average [37] is used to estimate pressure PSD, which are the tool to evaluate and compare compressor noise generation. Hamming windowing is used at blocks with 50% overlap. The number of blocks is selected so as to obtain the frequency resolution closest to 150 Hz.

The acoustic analysis is performed dividing the spectra in two regions: planar wave range and high frequency range.

Planar wave range starts at lowest frequency attainable and finishes when the first asymmetric mode is cut on. In this range, numerical simulations require pressure decomposition to avoid the nodes of standing waves. Experimental signals are decomposed used the beamforming-based technique described by Piñero et al. [36], although it imposes a constraint on maximum frequency [34]. Pressure components from the simulations are obtained by means of Eqn. 3:

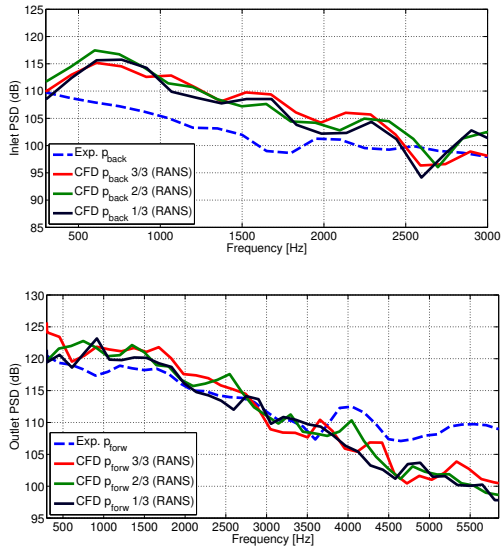

Figure 8: Low frequency PSD of experimental and URANS pressure components at inlet (top) and outlet (bottom) ducts.

$$p_{forw} = p_{ref}\left[\frac{1}{2}\left(1+\left(\frac{p}{p_{ref}}\right)^{\frac{\gamma-1}{2\gamma}}\left(1+\frac{\gamma-1}{2}\frac{u}{a}\right)\right)\right]^{\frac{2\gamma}{\gamma-1}} \tag{3}$$

$$p_{back} = p_{ref}\left[\frac{1}{2}\left(1+\left(\frac{p}{p_{ref}}\right)^{\frac{\gamma-1}{2\gamma}}\left(1-\frac{\gamma-1}{2}\frac{u}{a}\right)\right)\right]^{\frac{2\gamma}{\gamma-1}}$$

which are inspired by the Method of Characteristics (MoC), as described by Torregrosa et al. [38]. Flow field variables are averaged at cross-sections.

High frequency range starts with the onset of first asymmetric mode and is extended until 20 kHz. Point monitors located at wall ducts should be used in this frequency range so as to capture higher order acoustic modes [34]. Eq. 3 is again used to obtain the numerical spectra of pressure components in order to reduce the impact of standing waves, whereas beamforming cannot be applied to experimental pressure traces and thus a single probe of each array is used to obtain the raw PSD.

In this way, Figs. 8–11 are obtained. URANS and detached-eddy simulations were performed using the configuration described in Section 3.1.

Figures 8 and 9 show that, at the inlet, experimental spectrum at low frequency range decays monotonously. Inlet numerical spectra is predicted by both turbulence approaches alike. Simulations also provide decreasing spectra, but amplitude is overpredicted. Moreover, TCR does not have an impact on PSD.

At the outlet duct, experimental spectrum decreases until 3.5 kHz, presenting a narrow band noise and a constant level afterwards. URANS PSD depicted in Fig. 8 fails to predict this change in behavior, showing a constant decay for all TCRs. Conversely, DES spectra (Fig. 9) does present a narrow band centered at a frequency from 3.5 to 4 kHz, depending on tip clearance. Then, PSD are constant. The only difference between DES spectrum and experimental one is the broad band that simulations predict from 1.3 kHz to 2.5 kHz. It corresponds to the whoosh noise phenomenon detected at experiments for higher mass flows (see Broatch et al. [34]).

The differences in spectra prediction between turbulence approaches increase when frequencies above planar-wave range are considered. Figure 10 presents spectra provided by URANS simulation against experimental ones. At the inlet, the broadband elevation from 5 to 12 kHz is clearly underpredicted, showing a better agreement in the subsequent decay. PSD at the

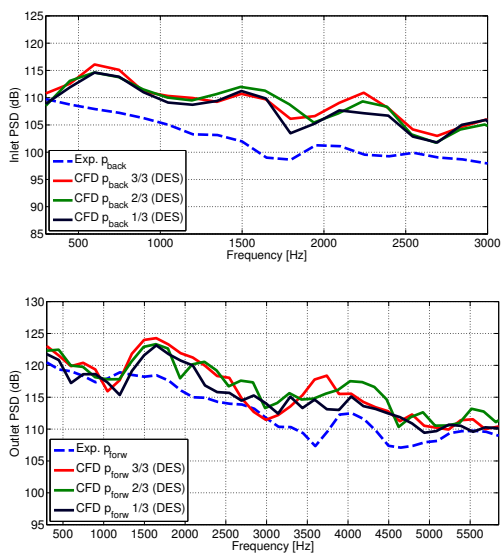

Figure 9: Low frequency PSD of experimental and DES pressure components at inlet (top) and outlet (bottom) ducts.

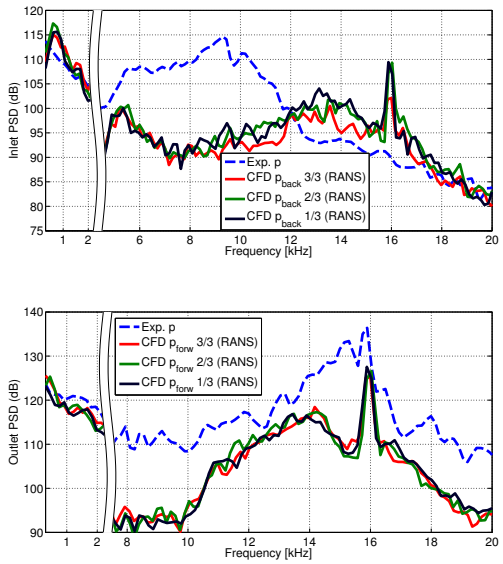

Figure 10: High frequency PSD of experimental and URANS pressure at inlet (top) and outlet (bottom) ducts.

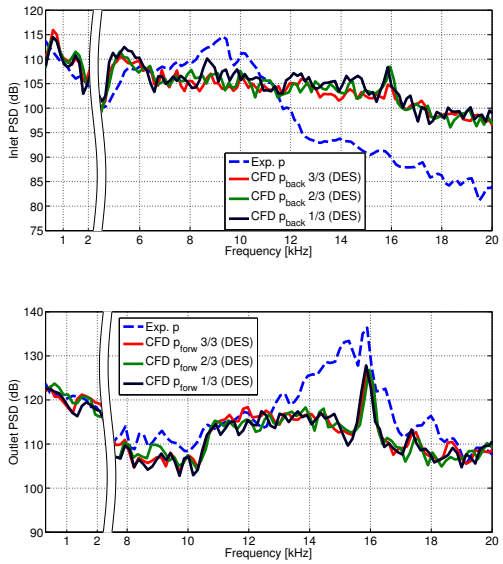

Figure 11: High frequency PSD of experimental and DES pressure at inlet (top) and outlet (bottom) ducts.

outlet duct is underpredicted, particularly for frequencies below 10 kHz.

DES (Fig. 11) provides an inlet spectrum with a closer estimation of the mean amplitude during the broadband elevation, although it fails to predict PSD decrease above 12 kHz. The narrow band between 4.7 and 6 kHz is not registered by the experimental measurement. At the outlet duct, PSD is accurately reproduced using the DES, save for a broadband elevation from 14 to 16 kHz that the experiments include.

Even though planar wave spectra predictions for both turbulence approaches are alike, DES shows superior performance at high frequencies. Only inlet spectrum above 12 kHz is overpredicted, and it does not represent a major issue since inlet PSD is significantly lower than outlet one (average of 10 dB), and human hearing sensitivity from 12 kHz onwards is limited.

5. Flow field investigation

In this section, flow field is investigated to explain why TCR is not relevant to compressor noise generation in these near-surge operating conditions (mass flow rate is 1.4 times surge mass flow at the speed line of 160 krpm). Only detached-eddy simulations are analyzed, since Section 4.3 has confirmed their (slightly) superior performance over URANS in terms of noise prediction.

Figure 12 shows the mean flow field for the cases with different tip clearance. The different fluid variables have been time-averaged during more than 10 impeller rotations. Line Integral Convolution (LIC) [39] is used to represent relative velocity vectors as an oil flow over isomeridional surfaces depicted in Fig. 6. These surfaces of revolution have been flattened by projecting them on a normalized-meridional vs. circumferential plane [40]. In Fig. 12, LIC is blended with pressure contours.

The impeller rotation is transformed into a horizontal translation from right to left in Fig. 12. Therefore, the left side of the blades corresponds to the PS whereas the right side is the SS, as confirmed by pressure contours. The solid black line shown in Fig. 12 represents a change of sign of meridional component of velocity. The majority of the impeller isomeridional section presents incoming flow, save for the vicinity of the shroud, in which backflow appear. Since tip clearance is included in this recirculating region, tip leakage flow is not only driven by favorable pressure gradient across the blade tip.

In order to shed some light on tip leakage flow, Fig. 13 shows the flow field at isomeridional surface number 3 (see Fig. 6), for the three cases with

different tip clearance. Time-averaged flow field is considered in the left side pictures, whereas the pictures on the right side represent a snapshot of the instantaneous flow. In addition to oil flow colored by pressure and a solid black line indicating zero meridional velocity, as in Fig. 12, relative velocity vectors are depicted. It can be seen that some of these vectors indicate flow going to the SS of the passages, i.e., there are cells with relative velocity oriented in the rotational direction. The region in which relative tangential velocity points to the left is highlighted and delimited by a solid violet line in Fig. 13.

Left side of Fig. 13 shows that the time-averaged flow goes in the streamwise direction and moves from SS to PS at the inner core of the passages (close to the hub). Conversely, flow is going backwards near the shroud as already noted, and a fraction of this recirculating flow goes from passage PS to SS. In the shroud boundary layer, absolute velocity is close to zero, so relative tangential velocity points to the right. These changes in circumferential flow direction results in the creation of secondary flows, such as the vortices observed in Fig. 13. Vortex cores are usually regions with local minimum of pressure (see for instance the instantaneous flow for the case with 1/3 of the original clearance).

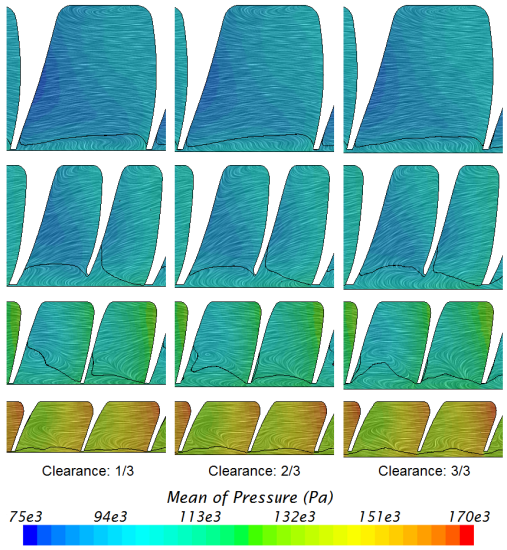

Figure 12: LIC of relative velocity vectors colored by pressure at isomeridional surfaces for DES cases with different clearance. Zero meridional velocity is represented as a solid black line.

The air flowing in two opposite directions in the tip clearance that can be observed in the right side of Fig. 13 creates a strong shear stress in this region, thus disabling the inviscid character of tip leakage flow [41], at least for near-stall operating conditions. If tip leakage mechanism were mainly inviscid, tip clearance could be resolved with few spanwise nodes (less than 10) [42, 43]. In this paper, about 20 cells were used to mesh the spanwise direction of tip clearance (see Fig. 6). Van Zante et al. [44] already noted that tip grid can influence prediction of stall inception.

Left side of Fig. 13 indicates that mean tip leakage flow moves from the right to the left, and this is justified by the pressure gradient that exists at the different sides of the blade tip. However, if the snapshots at right side of Fig. 13 are considered, it can be noticed that instantaneous net tip flow can be oriented in the rotational direction. The reason of the unexpected behavior of tip leakage flow can be explained by Fig. 14, which depicts the mean flow in a meridional view at midpitch distance between main blade SS and splitter

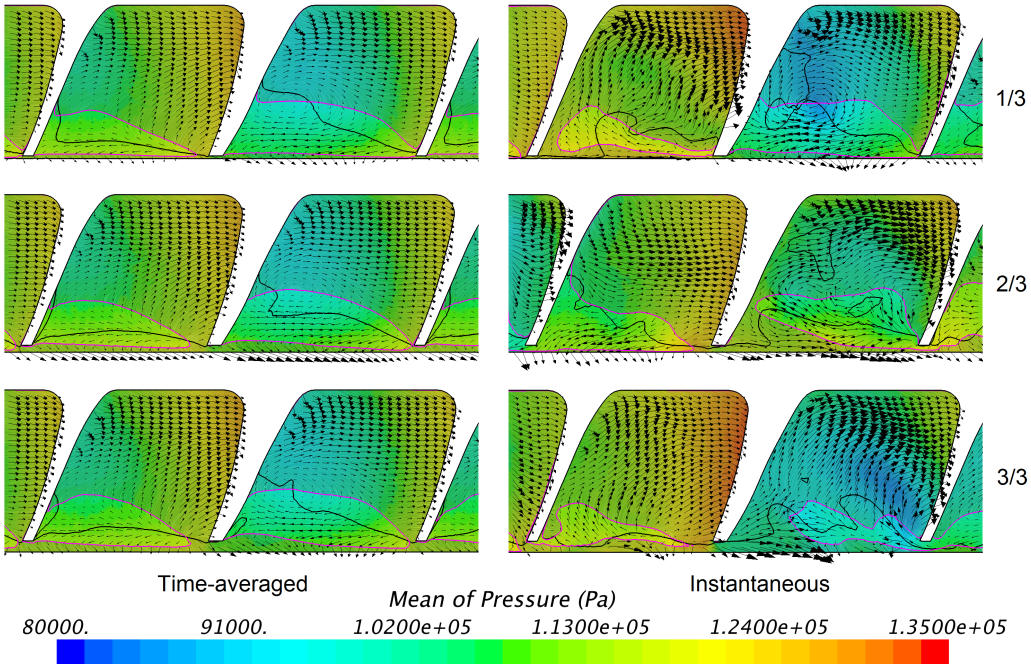

Figure 13: LIC of relative velocity vectors colored by pressure and relative velocity vectors glyph at isomeridional surface number 3 for DES cases with different clearance. Zero meridional velocity is represented as a solid black line whereas zero relative circumferential velocity is represented as a solid violet line.

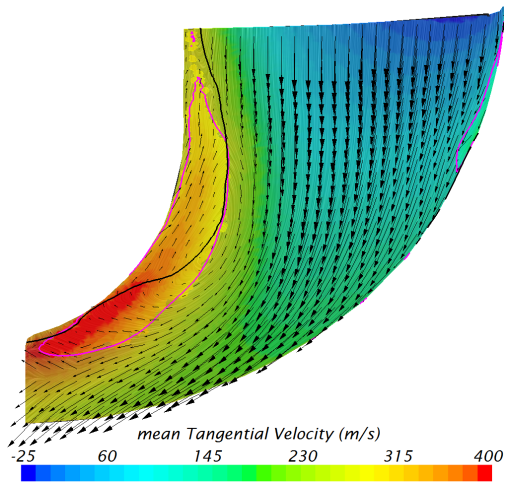

Figure 14: LIC of relative velocity vectors colored by tangential velocity and relative velocity vectors glyph at meridional surface for baseline clearance DES. Zero meridional velocity is represented as a solid black line whereas zero relative circumferential velocity is represented as a solid violet line.

blade PS. The solid black line representing change in meridional velocity direction shows that recirculating flow near the shroud almost extends to the trailing edge of the impeller for these operating conditions, although this conclusion could also be drawn from Fig. 12. Highest tangential velocities are obtained at the blade trailing edge, since it is the place where blade tip velocity is greatest. The backflow transports the angular momentum that the impeller transmitted to the flow when it was going in the streamwise direction. When the flow is reversed, it will lose some angular momentum because of the shear stress with the incoming flow, but also it will also gain tangential velocity, as radius is reduced.

Figure 14 shows that mean tangential velocity is in the order of blade tip velocity near the shroud, which explains the existence of regions in which relative velocity is oriented towards the passage SS (marked with a solid violet line in Fig. 14). Flow leaking from blade PS to SS through the tip is therefore diminished due to angular momentum of backflows. This fact may explain the reduction of clearance flow rate detected by Liu et al. [45] as operating condition is shifted towards surge.

Some researchers have studied tip clearance noise (TCN), which is attributed to jet-like tip leakage flow, the roll-up of this stream into a vortex and the interaction of these phenomena with adjacent blades [46]. TCN has

been thoroughly investigated in axial turbomachinery [47, 48], but it is not so well know in the case of radial turbomachinery. Raitor and Neise [3] reported a narrow band noise in a centrifugal compressor that was considered as TCN because it presented similarities to the case of axial turbomachinery. Bousquet et al. [49] found a periodic vortex shedding due to tip leakage flow in their simulation of a centrifugal compressor at near stall conditions, which may produce a narrow band noise. However, no recirculating flow appeared near the compressor shroud.

In order to produce a narrow ban noise, tip vortex shedding should occur in a freestream flow without any other strong fluctuating phenomena. For the operating conditions studied in this paper, the whole tip is immersed in the recirculating region, which would mask any noise that may produce tip leakage or even disable the noise source mechanisms. In the simulations, it could not be found any periodic tip vortex shedding nor acoustic fluctuations that could be related to tip leakage flow. Only rotating stall was found, but it is a subsynchronous phenomenon that produces the so-called whoosh noise (see the work of Broatch et al. [50]), and according to Figs. 8–11 TCR does not affect whoosh noise neither. The modification of tip leakage behavior due to the existence of a strong swirling recirculating flow near the shroud is the proposed mechanism to explain that noise generated by the centrifugal compressor is not affected by TCR, at least for the near-stall operating conditions studied in this paper.

6. Concluding remarks

In this paper, tip clearance sensitivity to flow field and noise generation of a 49 mm exducer diameter centrifugal compressor has been investigated. Measurements of turbocharger shaft motion show that, for a compressor speed of 160 krpm, tip clearance can be modified by a factor of 22% to 34%. FEM predicts that temperature and rotation cause an additional tip clearance reduction of 11%.

3D CFD simulations with three different tip clearance levels show that clearance reductions cause increases in pressure ratio and isentropic efficiency, but no significant changes in compressor acoustic signature. Two different turbulence approaches (URANS and DES) are studied, and DES is found to provide spectra with better agreement against experimental measurements, particularly at high frequencies (above onset of higher order acoustic modes).

Insensitivity of spectra to TCR is explained by flow field configuration. Since the working point is close to surge, the flow in the vicinity of the shroud is reversed and tip leakage flow is not only driven by pressure gradient at blade tip. A complicated flow pattern is detected in this region, but the recirculating flow comprises tip clearance. A coherent noise source mechanism due to tip leakage flow cannot be established, so variations of TCR do not have an impact on noise generation. Conversely, compressor performance indicators *are* affected by TCR, because tighter tip clearances lead to smaller backflow regions and reduced mixing losses.

These conclusions are valid for the studied operating conditions. Compressors working with higher mass flow rates should present less backflows close to the shroud and tip sensitivity to noise generation may be different. In any case, the present paper shows that, for operating conditions close to surge, researchers can rely on CAD tip clearance profile when analyzing acoustic behavior of centrifugal compressors.

Acknowledgements

The equipment used in this work has been partially supported by FEDER project funds "Dotación de infraestructuras científico técnicas para el Centro Integral de Mejora Energética y Medioambiental de Sistemas de Transporte (CiMeT), (FEDER-ICTS-2012-06)", framed in the operational program of unique scientific and technical infrastructure of the Ministry of Science and Innovation of Spain. The authors wish to thank Mr. Pau Raga for his worthy assistance during the meshing process.

References

References

[1] D. Evans, A. Ward, Minimizing Turbocharger Whoosh Noise for Diesel Powertrains, SAE Technical Paper 2005-01-2485. doi:10.4271/2005-01-2485.

[2] C. Teng, S. Homco, Investigation of Compressor Whoosh Noise in Automotive Turbochargers, SAE Int. J. of Passeng. Cars-Mech. Syst. 2 (1) (2009) 1345–1351. doi:10.4271/2009-01-2053.

List of Symbols

a	speed of sound	$m \cdot s^{-1}$
c_p	specific heat capacity at constant pressure	$J \cdot kg^{-1} \cdot K^{-1}$
$\dot{m}$	mass flow rate	$kg \cdot s^{-1}$
N	compressor rotational speed	rpm
p	pressure	Pa
t	time	s
T	temperature	K
u	axial velocity	$m \cdot s^{-1}$
$\dot{W}$	compressor absorbed power	$kg \cdot m^2 \cdot s^{-3}$
W_u	compressor specific work	$m^2 \cdot s^{-2}$
η	efficiency	%
ϵ	relative difference	%
γ	ratio of specific heats	$-$
ϕ	generic variable	
$\Pi_{t,t}$	total-to-total pressure ratio	$-$
τ	compressor torque	$kg \cdot m^2 \cdot s^{-2}$

Sub- and Superscripts

$*$	corrected variable
0	stagnation variable
1/3, 2/3, 3/3	related to one third, two thirds or three thirds of original clearance, respectively
$back$	backward travelling wave
CFD	related to simulation
exp	related to experimental measurement
in	inlet duct
$forw$	forward travelling wave
out	outlet duct
s	isentropic
ref	reference value

[3] T. Raitor, W. Neise, Sound generation in centrifugal compressors, Journal of Sound and Vibration 314 (2008) 738–756. doi:10.1016/j.jsv.2008.01.034.

[4] F. Mendonça, O. Baris, G. Capon, Simulation of Radial Compressor Aeroacoustics using CFD, in: Proceedings of ASME Turbo Expo

List of abbreviations

BPF	blade passing frequency
CAD	computer-aided design
CFD	computational fluid dynamics
DDES	delayed DES
DES	detached eddy simulation
FEM	finite element method
IDDES	improved DDES
LES	large eddy simulation
LIC	line integral convolution
MoC	Method of Characteristics
PS	(blade) pressure side
PSD	power spectral density
RANS	Reynolds-averaged Navier-Stokes
TCN	tip clearance noise
TCR	tip clearance ratio
SS	(blade) suction side
URANS	Unsteady RANS
WMLES	wall-modeled LES

2012, no. GT2012-70028, ASME, 2012, pp. 1823–1832. doi:10.1115/GT2012-70028.

[5] I. Tomita, S. Ibaraki, M. Furukawa, K. Yamada, The Effect of Tip Leakage Vortex for Operating Range Enhancement of Centrifugal Compressor, Journal of Turbomachinery 135 (5) (2013) 8. doi:10.1115/1.4007894.

[6] S. N. Danish, M. Chaochen, Y. Ce, L. Wei, Comparison of Two Methods to Increase the Tip Clearance and its Effect on Performance of a Turbocharger Centrifugal Compressor Stage, in: International Conference on Energy and Environment, 2006, p. 7.

[7] Y. Jung, M. Choi, S. Oh, J. Baek, Effects of a nonuniform tip clearance profile on the performance and flow field in a centrifugal compressor, International Journal of Rotating Machinery 2012. doi:10.1155/2012/340439.

[8] H.-L. Wang, G. Xi, J.-Y. Li, M.-J. Yuan, Effect of the tip clearance vari-

ation on the performance of a centrifugal compressor with considering impeller deformation, Proceedings of the Institution of Mechanical Engineers, Part A: Journal of Power and Energy 225 (8) (2011) 1143–1155. doi:10.1177/0957650911416914.

[9] F. Nelson, Rotordamics without equations, International Journal of COMADEM 10 (3) (2007) 2–10.

[10] T. Sotome, S. Sakoda, Development of Manufacturing Technology for Precision Compressor Wheel Castings for Turbochargers, Furukawa Review 32 (2007) 56–59.
URL https://www.furukawa.co.jp/review/fr032.htm

[11] J. V. Pastor, J. R. Serrano, V. Dolz, M. A. López, F. Bouffaud, Study of turbocharger shaft motion by means of non-invasive optical techniques: Application to the behaviour analysis in turbocharger lubrication failures, Mechanical Systems and Signal Processing 32 (2012) 292–305. doi:10.1016/j.ymssp.2012.04.020.

[12] J. V. Pastor, J. R. Serrano, V. Dolz, M. A. López, A Non-invasive Optical Technique to Observe Turbocharger Shaft Whirl, in: XXI Biennial Symposium on Measuring Techniques in Turbomachinery, 2012, iSBN: 978-84-8363-966-5.

[13] J. Galindo, J. Serrano, V. Dolz, M. López, Behavior of an IC Engine Turbocharger in Critical Condition of Lubrication, SAE International Journal Engines 6. doi:10.4271/2013-01-0921.

[14] M. López, Estudio Teórico-Experimental de la Dinámica Rotacional de Turbocompresores de MCIA. Aplicación al diagnóstico de fallos., Ph.D. thesis, Universitat Politècnica de València (2014).

[15] R. Navarro, A numerical approach for predicting flow-induced acoustics at near-stall conditions in an automotive turbocharger compressor, Ph.D. thesis, Universitat Politècnica de València (2014).
URL http://hdl.handle.net/10251/44114

[16] C. A. Wagner, T. Hüttl, P. Sagaut (Eds.), Large-Eddy Simulation for Acoustics, Cambridge University Press, 2007.

[17] G. Dufour, N. Gourdain, F. Duchaine, O. Vermorel, L. Gicquel, J. F. Boussuge, T. Poinsot, Large eddy simulation applications, in: Numerical Investigations in Turbomachinery: A State of the Art, VKI Lecture Series, 2009.

[18] A. Karim, K. Miazgowicz, B. Lizotte, A. Zouani, Computational aero-acoustics simulation of compressor whoosh noise in automotive turbochargers, SAE Technical Paper 2013-01-1880. doi:10.4271/2013-01-1880.

[19] F. Hellström, E. Guillou, M. Gancedo, R. DiMicco, A. Mohamed, E. Gutmark, L. Fuchs, Stall Development in a Ported Shroud Compressor using PIV Measurements and Large Eddy Simulation, Tech. rep., SAE Technical Paper 2010-01-0184 (2010). doi:10.4271/2010-01-0184.

[20] F. Hellstrom, E. Gutmark, L. Fuchs, Large Eddy Simulation of the Unsteady Flow in a Radial Compressor Operating Near Surge, Journal of turbomachinery 134 (5). doi:10.1115/1.4003816.

[21] V. Jyothishkumar, M. Mihaescu, B. Semlitsch, L. Fuchs, Numerical flow analysis in centrifugal compressor near surge condition, in: Fluid Dynamics and Co-located Conferences, American Institute of Aeronautics and Astronautics, 2013, p. 13. doi:10.2514/6.2013-2730.

[22] B. Semlitsch, V. JyothishKumar, M. Mihaescu, L. Fuchs, E. Gutmark, M. Gancedo, Numerical Flow Analysis of a Centrifugal Compressor with Ported and without Ported Shroud, SAE Technical Paper 2014-01-1655. doi:10.4271/2014-01-1655.

[23] F. R. Menter, Two-equation eddy-viscosity turbulence models for engineering applications, AIAA journal 32 (8) (1994) 1598–1605.

[24] F. R. Menter, R. Langtry, T. Hansen, CFD simulation of turbomachinery flows–verification, validation and modeling, in: European Congress on Computational Methods in Applied Sciences and Engineering, ECCOMAS, 2004.

[25] C. Robinson, M. Casey, B. Hutchinson, R. Steed, Impeller-diffuser Interaction in Centrifugal Compressors, in: Proceedings of ASME Turbo Expo 2012, no. GT2012-69151, ASME, 2012.

[26] P. E. Smirnov, T. Hansen, F. R. Menter, Numerical Simulation of Turbulent Flows in Centrifugal Compressor Stages With Different Radial Gaps, in: Proceedings of GT2007, no. GT2007-27376, ASME, 2007. doi:10.1115/GT2007-27376.

[27] P. G. Tucker, Computation of unsteady turbomachinery flows: Part 2–les and hybrids, Progress in Aerospace Sciences 47 (7) (2011) 546–569. doi:10.1016/j.paerosci.2011.07.002.

[28] Detached-eddy simulations past a circular cylinder, Flow, Turbulence and Combustion 63 (1-4) (2000) 293–313.

[29] A. K. Travin, M. L. Shur, P. R. Spalart, M. K. Strelets, Improvement of delayed detached-eddy simulation for les with wall modelling, in: European Conference on Computational Fluid Dynamics (ECCOMAS CFD 2006), 2006.

[30] M. L. Shur, P. R. Spalart, M. K. Strelets, A. K. Travin, A hybrid RANS-LES approach with delayed-DES and wall-modelled LES capabilities, International Journal of Heat and Fluid Flow 29 (6) (2008) 1638–1649. doi:10.1016/j.ijheatfluidflow.2008.07.001.

[31] C. Mockett, A comprehensive study of detached-eddy simulation, Ph.D. thesis, Technische Universität Berlin (2009).

[32] R. van Rennings, K. Shi, S. Fu, F. Thiele, Delayed-detached-eddy simulation of near-stall axial compressor flow with varying passage numbers, in: S. Fu, W. Haase, S.-H. Peng, D. Schwamborn (Eds.), Progress in Hybrid RANS-LES Modelling, Vol. 117 of Notes on Numerical Fluid Mechanics and Multidisciplinary Design, Springer Berlin Heidelberg, 2012, pp. 439–448. doi:10.1007/978-3-642-31818-4_38.

[33] CD-adapco, STAR-CCM+, release version 8.04.007 Edition (June 2013). URL http://www.cd-adapco.com

[34] A. Broatch, J. Galindo, R. Navarro, J. García-Tíscar, Methodology for experimental validation of a CFD model for predicting noise generation in centrifugal compressors, International Journal of Heat and Fluid Flow 50 (2014) 134–144. doi:10.1016/j.ijheatfluidflow.2014.06.006.

[35] J. Galindo, J. Serrano, C. Guardiola, C. Cervelló, Surge limit definition in a specific test bench for the characterization of automotive turbochargers, Experimental Thermal and Fluid Science 30 (5) (2006) 449–462. doi:10.1016/j.expthermflusci.2005.06.002.

[36] G. Piñero, L. Vergara, J. Desantes, A. Broatch, Estimation of velocity fluctuation in internal combustion engine exhaust systems through beamforming techniques, Measurement Science & Technology 11 (11) (2000) 1585–1595. doi:10.1088/0957-0233/11/11/307.

[37] P. Welch, The use of fast fourier transform for the estimation of power spectra: a method based on time averaging over short, modified periodograms, Audio and Electroacoustics, IEEE Transactions on 15 (2) (1967) 70–73.

[38] A. J. Torregrosa, P. Fajardo, A. Gil, R. Navarro, Development of a non-reflecting boundary condition for application in 3D computational fluid dynamic codes, Engineering Applications of Computational Fluid Mechanics 6 (3) (2012) 447–460.

[39] B. Cabral, L. C. Leedom, Imaging vector fields using line integral convolution, in: Proceedings of the 20th annual conference on Computer graphics and interactive techniques, ACM, 1993, pp. 263–270.

[40] M. Drela, H. Youngren, A User's Guide to MISES 2.63, MIT Aerospace Computational Design Laboratory (2008).

[41] J. A. Storer, N. A. Cumpsty, Tip Leakage Flow in Axial Compressors, Journal of Turbomachinery 113 (2) (1991) 252–259. doi:10.1115/1.2929095.

[42] H.-J. Eum, Y.-S. Kang, S.-H. Kang, Tip clearance effect on throughflow and performance of a centrifugal compressor, KSME International Journal 18 (6) (2004) 979–989. doi:10.1007/BF02990870.

[43] Shum, Yu Kwong Patrick and Cumpsty, N. A. and Tan, C. S., Impeller–diffuser interaction in a centrifugal compressor, Journal of Turbomachinery 122 (4) (2000) 777–786. doi:10.1115/1.1308570.

[44] D. E. Van Zante, M. D. Hathaway, T. H. Okiishi, A. J. Strazisar, J. R. Wood, Recommendations for Achieving Accurate Numerical Simulation

of Tip Clearance Flows in Transonic Compressor Rotors, Journal of turbomachinery 122 (4) (2000) 733–742. doi:10.1115/1.1314609.

[45] Z. Liu, Y. Ping, M. Zangeneh, On the nature of tip clearance flow in subsonic centrifugal impellers, Science China Technological Sciences 56 (9) (2013) 2170–2177. doi:10.1007/s11431-013-5313-3.

[46] M. C. Jacob, J. Grilliat, R. Camussi, G. C. Gennaro, Aeroacoustic investigation of a single airfoil tip leakage flow, International Journal of Aeroacoustics 9 (3) (2010) 253–272.

[47] T. Fukano, C.-M. Jang, Tip clearance noise of axial flow fans operating at design and off-design condition, Journal of sound and vibration 275 (3) (2004) 1027–1050. doi:10.1016/S0022-460X(03)00815-0.

[48] F. Kameier, W. Neise, Experimental study of tip clearance losses and noise in axial turbomachines and their reduction, Journal of turbomachinery 119 (3) (1997) 460–471.

[49] Y. Bousquet, X. Carbonneau, G. Dufour, N. Binder, I. Trebinjac, Analysis of the Unsteady Flow Field in a Centrifugal Compressor from Peak Efficiency to Near Stall with Full-Annulus Simulations, International Journal of Rotating Machinery 2014 (2014) 11. doi:10.1155/2014/729629.

[50] A. Broatch, J. Galindo, R. Navarro, J. García-Tíscar, A. Daglish, R. K. Sharma, Simulations and measurements of automotive turbocharger compressor whoosh noise, Engineering Applications of Computational Fluid Mechanicsdoi:10.1080/19942060.2015.1004788.